Received: 4 March 2021 | Revised: 11 October 2021 | Accepted: 7 December 2021

DOI: 10.1049/tje2.12127

The Journal of Engineering

The Institution of Engineering and Technology WILEY

ORIGINAL RESEARCH

Lessening gap loss concentration problems in nanocrystalline cores by alloy gap replacement

Xuan Guo[1] | **Li Ran**[1,2] | **Peter Tavner**[3]

[1] School of Engineering, University of Warwick, Coventry, UK

[2] School of Electrical Engineering, University of Chongqing, Chongqing, China

[3] School of Engineering and Computing Sciences, Durham University, Durham, UK

Correspondence
Xuan Guo, School of Engineering, University of Warwick, Coventry, CV4 7AL, UK
Email: X.guo.5@warwick.ac.uk

Abstract

A simple method is proposed here to improve the gap loss concentration problem of a nanocrystalline core in an LCL filter inductor for high switching frequency converters using SiC devices. This alloy-gapped inductor design aims to reach two primary goals. First, to reduce the concentrated gap loss in a nanocrystalline core. Second, decrease the maximum temperature around the gap region and lead to more even temperature distribution. A finite element (FE) power loss and thermal models, validated by experiment, have been created to evaluate the proposed design. Based on the FE model results, the eddy current loss on the surfaces, which used to have the most severe gap loss is reduced by either 70% or 40% for the two commonly used winding placements. The total eddy current loss can be reduced by 29% and 27% for those two winding placements. In addition, FEA thermal model indicates that the hotspot temperature can be significantly decreased, and the nanocrystalline core can achieve a more uniform temperature distribution by this design, which can be a potential downsize method for the nanocrystalline core inductor.

1 | INTRODUCTION

Increasing power density is always one of the main targets for power converters. Since passive components account for a tremendous amount of the weight or volume of some power converter, then downsizing of magnetic components in power converters is always a promising method to increase the power density [1].

With the popularity of wide bandgap devices such as SiC power electronics, the increased switching frequency for power converters can reduce the inductor size. Meanwhile, for high-frequency inductor design, the use of nanocrystalline cores is also considered a potential method for downsizing the inductor due to its higher saturation magnetic flux density and lower core loss compared to commonly used ferrites. Furthermore, air gaps are necessary for high permeability core material such as nanocrystalline cores. The fringing flux caused by the air gaps induces eddy current loss in the outermost lamination layers around the gap region, which accounts for a tremendous core loss and causes localized hotspots on the gap region, which dominate the internal temperature. Since the size of magnetic components is mainly thermally limited, the localized hotspot caused by the concentrated gap loss can affect the downsize of the nanocrystalline core-based inductor design and may damage the insulation layers [2]. Hence, reducing hotspot temperature is the primary key for nanocrystalline core inductor size reduction. This eddy current loss has been thoroughly characterized in [3–5] for high-frequency and high-current DC inductors. Meanwhile, Figure 1 indicates that the current through the filter inductor consists of a 50 Hz sinusoidal current and a high frequency, high magnitude ripple current. The 50 Hz current can be regarded as DC current. Therefore, the eddy current loss concentration problem in the filter inductor is easy to be predicted as dc inductors. For capitalizing better on nanocrystalline cores and SiC devices in converters, a proper method needs to be implanted to reduce the gap loss concentration problem.

Adding discrete air gaps is always a promising method to reduce the effects of fringing flux on the winding loss and core loss [6]. Moreover, reshaping the air gaps can also achieve the same purpose [7]. Besides the manufacturing difficulties, the above methods both may cause short-circuit problems due to the thin metal ribbon of the nanocrystalline cores. Ref. [8] examined the effects of air gap placements to decrease the

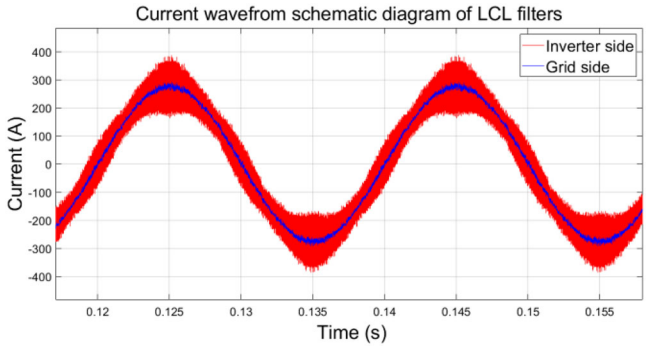

FIGURE 1 Typical current waveform of LCL filter inductors

corresponding power loss. Open-circuited copper screens and optimizing the air gap shape have been discussed in [9] and [10], respectively. However, those methods reduce the effects on winding loss instead of core loss, which are not useful for nanocrystalline cores.

Different magnetic material attachment can reduce the fringing flux, which can mitigate the concentrated gap loss [4, 11, 12]. However, the ferrite plat attachment limits the saturation point of the nanocrystalline cores. And the iron powder magnetic material is criticized due to high core loss and nonlinear saturation curve for high current, high-frequency DC inductor. Recent work revealed a nonlinear relation between the gap loss and those inductor parameters [2]. Therefore, the increased core loss from the alloy gap may be compensated by the reduced gap loss with proper inductor parameters. The extra core loss of the alloy gap is evenly distributed in the alloy, which does not lead to any localized hotspots. Hence, when reduced concentrated gap loss can be higher than the extra core loss from alloy, then hotspot temperature around the gap region can be decreased and uniform temperature distribution can be expected, which can lead to a significant inductor size reduction.

Here, the alloy gap replacement approach is applied to reduce concentrated gap loss and decrease the hotspot temperature and offer a more uniform temperature distribution. To examine the proposed method, accurate prediction of the eddy current loss distribution and thermal behaviour is necessary. Therefore, finite element (FEA) models have been developed and experimentally validated. The eddy current loss modelling, distribution and thermal distribution are based on FE models present in Sections 3 and 4. The corresponding experiments set up and FE model validation is illustrated in Section 5. Then the last section concludes the modelling results and performance of the proposed method and illustrates the future work.

2 | INDUCTOR DESIGN PROCEDURE

Obtaining the desired inductance and avoiding saturation is always the essential design factors for inductor design. The air gap is one of the critical factors to achieve these goals. When

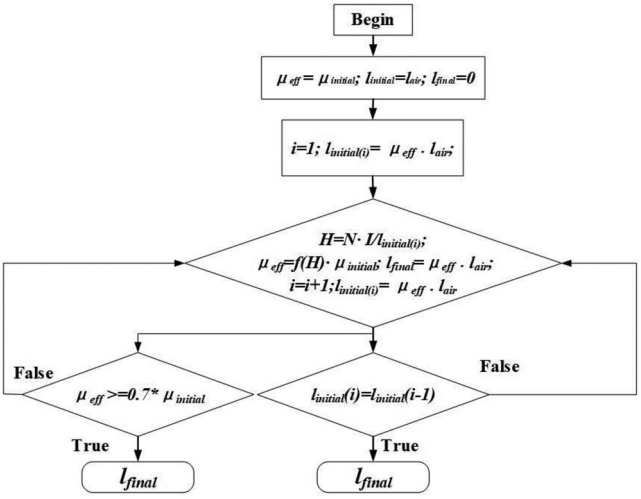

FIGURE 2 Flow chart of the gap length calculation

the two inductor designs share the same size and shape, then the cross-section and the mean length of both inductors are almost identical. Then the desired inductance means having a similar effective permeability based on the Equation (1):

$$L = \frac{\mu_{eff}\mu_0 N^2 A_c}{l_c} \tag{1}$$

where the μ_{eff} is the effective relative permeability of a non-gapped inductor; μ_0 is the permeability of free space; N is the winding turns. The l_c and the A_c represent the mean length and cross-section area of the core, respectively.

Furthermore, the same effective magnetic permeability also means the same magnetomotive force MMF, which is shown as [12]:

$$Ni = H_g l_g = \phi R_{eq} = \phi \frac{l_g}{\mu_{eff}\mu_0 A_g} \tag{2}$$

where i is the current through the coil; H_c is the magnetic field strength; ϕ is the magnetic flux; the effective reluctance of the magnetic circuit R_{eq} can be represented in At/wb.

However, the effective permeability of the alloy varies with the applied magnetic field strength H, which is related to the current through the coil when the size and shape are certain. Therefore, to calculate the proper alloy gap length, the function $f(H)$ between the relative permeability and the magnetic field strength of the alloy gap can be obtained by the datasheet first. Moreover, the alloy-gapped inductor does not vary much as the air-gapped inductor when close to the saturation limit. Therefore, the operating range should be within 70% of the saturation point of the inductor to ensure the desired inductance can be achieved within the operating range. The flow chart of the gap length calculation is displayed in Figure 2.

As for the alloy materials, the alloy replacement approach is to apply an alloy material whose magnetic permeability higher than

TABLE 1 Inductor core parameters

Inductor core parameters	Air gap	Alloy gap
The mean length of a closed magnetic core (mm)	334.2	304.2
Cross section area (mm^2)	900	900
Winding turns	10	10
Single Gap length (mm)	0.6	15

air and lower than the core materials to reduce the magnetic flux leakage around the air gap region. Hence, different permeability means different alloy gap length to achieve the same inductance as the air-gapped design. There are various kinds of iron powder magnetic materials with different characteristics. Since reducing the concentrated eddy current loss around the gap region is one of the primary targets, the alloy material with a lower core loss per unit volume at high frequency operating conditions is the desirable selection. Since further experimental confirmation is necessary, then the block shape of the chosen alloy material needs to be commercially available for experimental validation. Hence, the koolmu material is chosen as the alloy gap material due to relative low core loss and block shape is available. Other materials such as koolmu HF (high frequency), which has a lower core loss per unit volume, can be considered as a potential alternative when it has a commercially available block shape.

Furthermore, to minimize the interference of other inductor parameters on the comparison between two inductor designs, the alloy-gapped inductor maintains the same size and shape as the air-gapped inductor, as shown in Table 1. As for the desired inductance, the inductance value between two inductor designs with different inductor parameters is listed in Figure 3. It indicates that the alloy gapped inductor can obtain the same inductance as the traditional design under rated operating condition.

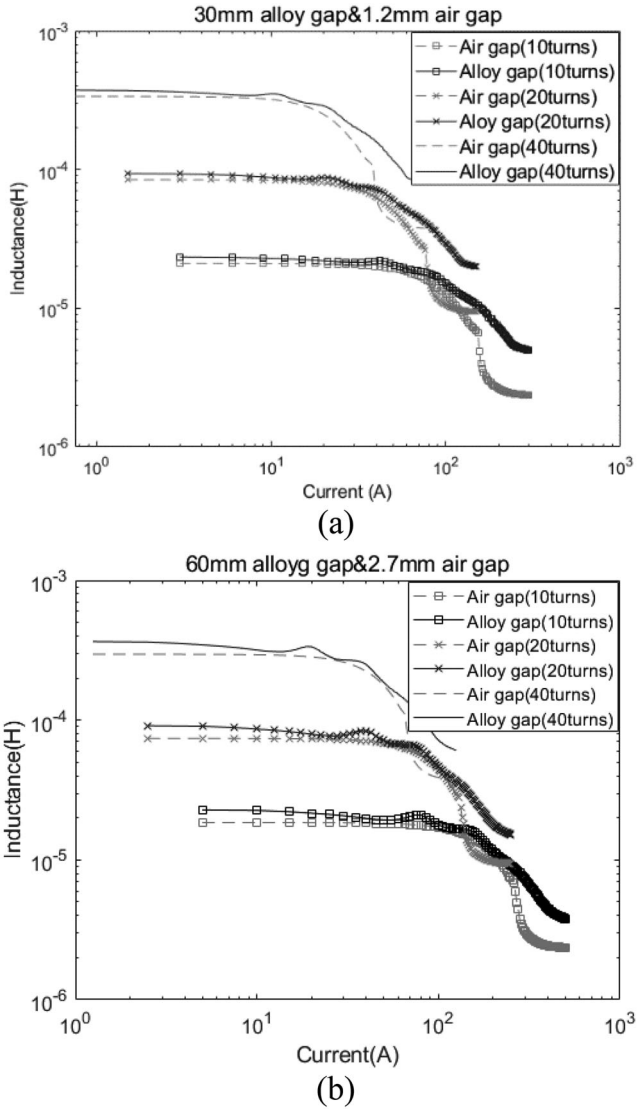

FIGURE 3 Inductance of different gap lengths and winding turns (a) short gap length (b) longer gap length

3 | FINITE ELEMENT POWER LOSS MODELLING

The FE models are developed and solved in COMSOL Multiphysics software. The inductor used in the FE models and experiments consists of two commonly used U type core with lize wire windings and the inductor structures are presented in Figure 4. The size of both inductors maintains the same to evaluate the effect of the proposed approach. The inductor parameters are specified in Table 1. Moreover, different winding placements have different magnetic flux leakage, which affects the fringing flux. Hence, two winding positions are involved in analysing the power loss distribution and thermal behaviours of both inductor designs in the FE models. When the winding is away from the gap, then the magnetic flux components, which are normal to the outermost lamination surfaces, increase. Hence, all the comparisons in the FEA modelling are based on two different winding positions.

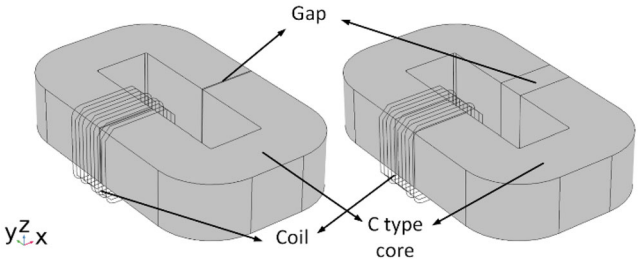

FIGURE 4 Inductor structure

3.1 | Homogenized approach

The fine thickness of the laminated nanocrystalline core is between 15–20 μm, which is unrealistic for direct layer-by-layer modelling. Hence, an alternative method is necessary for FEA modelling. The homogenized model has been considered as a

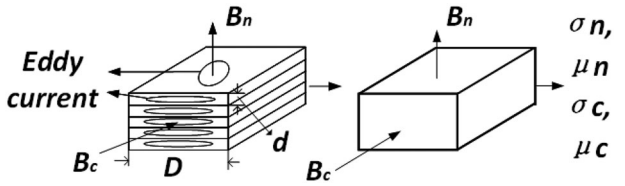

FIGURE 5 Schematic diagram of the anisotropic model

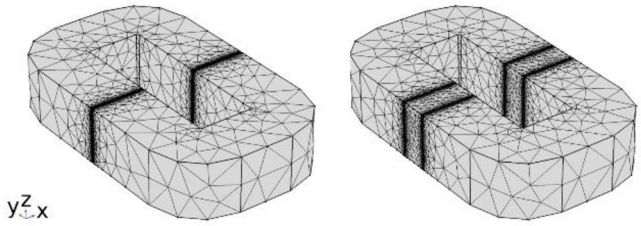

FIGURE 6 FEA mesh schematic diagram of air-gapped (left) and alloy-gapped inductor (right)

simple method to simplify the model and shorten the computation time for eddy current analysis in laminated cores [5, 13–16]. Moreover, among different homogenized modelling approaches, the model from [13] can be applied in a high-frequency environment and obtain comparable results with the direct method. The laminated core is introduced as a solid continuum with anisotropic electrical and magnetic parameters in the model shown in Figure 5. σ_c, μ_c, σ_n and μ_n are the electrical conductivity and magnetic permeability in corresponding directions. Based on the practical design, the stacking factor of the lamination layers, F, is set as 0.8; The equivalent conductivity and permeability of the laminated cores can be derived in Equations (7)–(9) [13].

Meanwhile, to obtain a reasonable computation time and a good accuracy, the FE mesh should be appropriately set. Hence, in a high-frequency operating environment, the effective skin depth should be considered in the FE power loss model and can be calculated as:

$$\delta_e = \sqrt{\frac{2}{\omega \mu_n \mu_0 \sigma_c}} \tag{3}$$

where ω is the angular frequency of the magnetisation current. μ_0 is the permeability of free space, which is set as 1.

Therefore, the minimum mesh size of the edges is set at 0.5 mm, which is around one-fourth of the skin depth of 20 kHz for accurate FE results. The rest region of both inductor cores is set as normal size mesh to achieve a reasonable computation time for both inductor models. The mesh structures of both inductor models are shown in Figure 6.

$$\mu_c = F \cdot \mu_m + (1 - F) \cdot \mu_0 \tag{4}$$

$$\mu_n = \frac{\mu_m \cdot \mu_0}{F \cdot \mu_0 + (1 - F) \cdot \mu_m} \tag{5}$$

TABLE 2 Equivalent anisotropic parameters of the FE model

Anisotropic parameters	Value
μ_c	80,000
μ_n	5
σ_c	6.67×10^5 (S/M)
σ_n	0.5 (S/M)

$$\sigma_c = F \cdot \sigma_m \tag{6}$$

$$\sigma_n = \left(\frac{d}{D}\right)^2 \cdot \frac{\sigma_m}{F} \tag{7}$$

where d and D are the thickness and width of a single lamination layer, which are 20 μm and 30 mm, respectively, in this model, based on the manufacture datasheet, the electrical conductivity σ_m, and the magnetic permeability μ_m of the nanocrystalline core are approximately 8.3×10^5 (S/M) and 10^5, respectively. Since the chosen alloy in this paper is iron powder material, which is a non-laminated structure, the electrical conductivity and magnetic permeability of the alloy gap are defined as 10 (S/M) and 26, respectively. The calculated anisotropic properties of the laminated core list in Table 2.

3.2 | Hysteresis loss and winding loss

The hysteresis loss only accounts for a small amount of core loss of the nanocrystalline core at a high frequency operating environment [2]. When most of the gap loss, which is the induced eddy current loss, concentrates around the gap region, especially the gap edges and cause localized hotspots, the hysteresis loss is evenly distributed in the whole core. Therefore, the hysteresis loss of both inductor designs is predicted from the datasheet of the manufactures instead of calculating in the models. The hysteresis loss can be derived based on an empirical equation [17]:

$$P_{m,sp} = k \cdot f^a (B_{ac})^b \tag{8}$$

where k, a and b are numerical constants that vary with different magnetic materials. $P_{m,sp}$ in mW/cm^3 when f is the operating or switching frequency in kHz and B_{ac} is the peak to peak ac magnetic flux density in mT.

Examining the proposed method performance to reduce the concentrated gap loss is the primary purpose of this paper. Moreover, the winding loss is also evenly distributed in the coil, which does not cause any localized hotspots on the core. Hence, the winding coil is set as a boundary current in the FE model and only considered as a magnetic source instead of a power loss source or heat source.

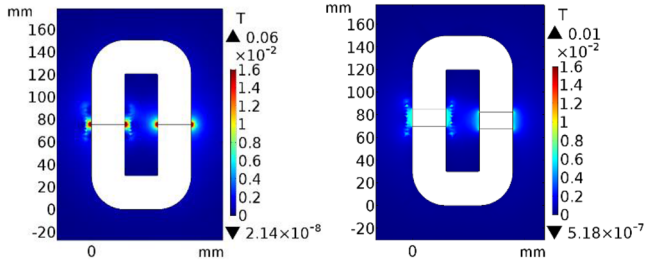

FIGURE 7 Magnetic flux density distribution in the air of the air gap (left) and the alloy gap (right) inductor design (winding at gap placement) ($I_{\text{pk–pk ripple}}$ = 32 A, Frequency = 20 kHz)

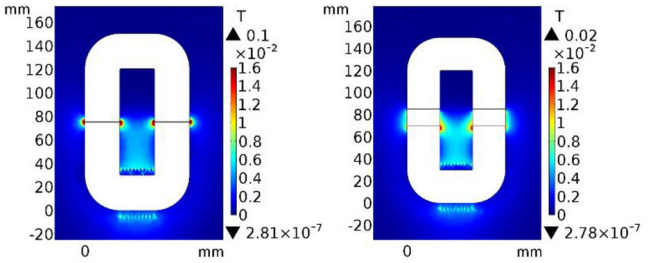

FIGURE 8 Magnetic flux density distribution in the air of the air gap (left) and the alloy gap (right) inductor design (winding at side placement) ($I_{\text{pk–pk ripple}}$ = 32A, Frequency = 20 kHz)

3.3 | Eddy current loss

In the FE models, the frequency study is often used for eddy current loss analysis in COMSOL software, which is chosen to model the eddy current loss distribution and loss calculation in this study. Furthermore, the eddy current loss can be calculated by integrating the volume and surface electromagnetic loss like the direct calculation methods. The SiC-based converter in the wind power system can operate at a switching frequency of 20 kHz. Hence, the operating frequency of the ripple current in this FEA model is set at 20 kHz to analysis the performance of the alloy gap method in the SiC converter. The eddy current loss calculation in FEA modelling can be expressed as:

$$P_e = \int_{\Omega} \sigma_{eq} E^2 d\Omega \tag{9}$$

where the σ_{eq} is the equivalent conductivity, E is the electric field. For the frequency study in COMSOL, eddy current loss is based on the relative magnetic permeability, which is set as a constant.

3.4 | Magnetic flux density distribution

Since the proposed method reduces the core loss and winding loss by minimizing the magnetic flux leakage, which is fringing flux, then the flux density distribution of both inductor designs needs to be examined.

The flux density distributions in Figures 7 and 8 are 3D FEA modelling results on the cut surfaces at the middle of the core. Only the flux density distribution in the air is displayed to illustrate the condition of the flux components, which are normal to the surface. Higher magnetic flux density means that there are more magnetic flux components normal to the lamination surface and higher potential corresponding eddy current.

Based on the results in Figures 7 and 8, the maximum flux density of the air-gapped inductor around the gap reaches 0.06 T with gap-winding placement, respectively and highly concentrate around the gap. However, for the alloy gapped inductor, the maximum flux density is only 0.01 T, which is only around 17% of the maximum flux density of the air-gapped inductor. For the side-winding position, the edges of the core and the alloy gap close to the coil appear to the high magnetic flux density points. The maximum flux density of the alloy gapped inductor is only 0.02, which is around 22% of the maximum flux density of the air-gapped inductor. Based on the magnetic flux density distribution results, the normal flux components around the gap position are greatly reduced by applying the alloy gap. Hence, concentrated eddy current loss caused by the flux normal to the lamination layers can be expected to achieve a considerable reduction. The comparisons of eddy current loss density distribution and power loss between two inductor designs present in the following section.

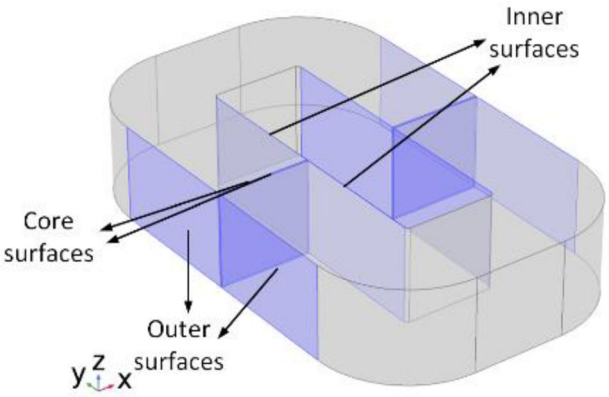

FIGURE 9 Inductor core surfaces with most severe gap loss

3.5 | Gap loss distribution

The induced eddy current loss concentrated around the gap region. However, due to the different electrical conductivity, the outer surfaces, inner surfaces, and the gap surfaces account for most of the gap loss, which presents in Figure 9 [2, 5]. Hence, the examination of the effect of the gap loss reduction of the proposed method focuses on those surfaces.

Based on the eddy current loss density comparison in Figure 10, while the peak-to-peak ripple current is 32 A, and the operating frequency is 20 kHz, the proposed alloy gap replacement can offer an order of magnitude reduction of the maximum eddy current loss density, which is from 2.39×10^7 to 2.56×10^6 W/m^3. The decrease is around 89% at gap-winding

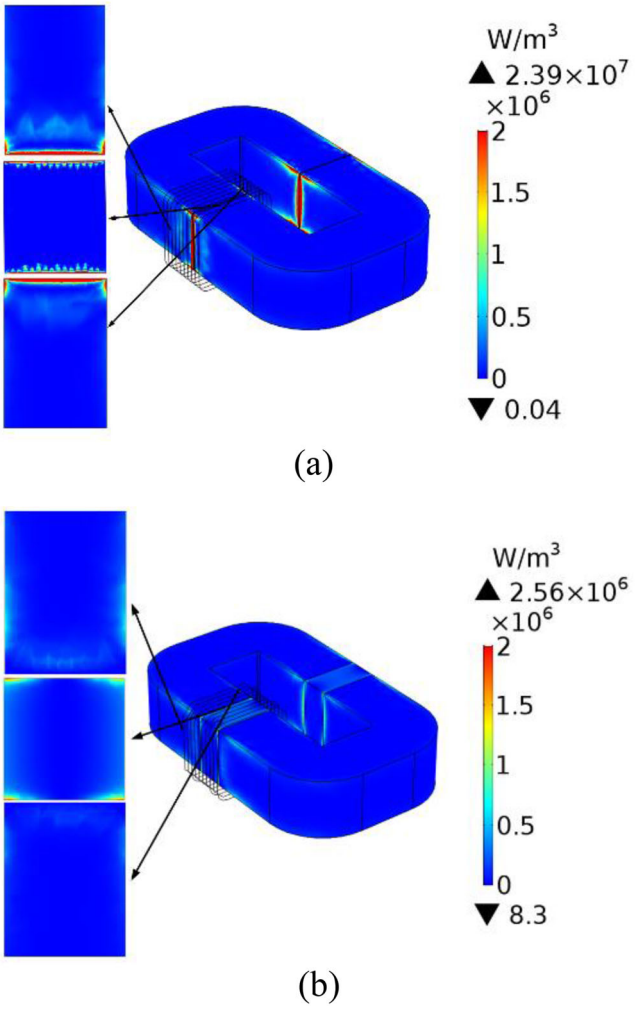

FIGURE 10 Comparison of eddy current loss distribution for the (a) air-gapped and (b) alloy gapped inductors (32 A peak-to-peak ripple current and 20 kHz) at gap winding placement

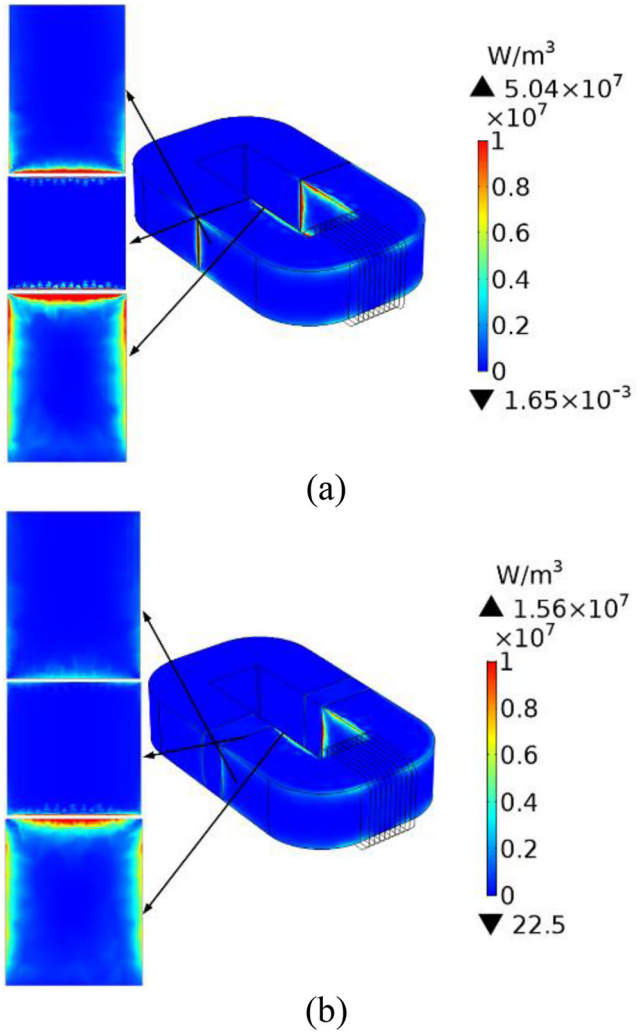

FIGURE 11 Comparison of eddy current loss distribution for the (a) air-gapped and (b) alloy gapped inductors (32 A peak-to-peak ripple current and 20 kHz) at side winding placement

placement. As for the side-winding placement, the maximum eddy current loss density can still be reduced from 5.04×10^7 to 1.56×10^7 W/m^3, which is about a 69% reduction. Furthermore, FE modelling results in Figures 10 and 11 both indicate that the alloy gap approach leads to a more uniform eddy current loss distribution. When it comes to higher frequency condition such as 40 kHz, the reduction of the maximum eddy current loss density can be reduced by 81%, which is from 7.2×10^7 to 1.31×10^7 W/m^3. In terms of side winding placement, the maximum eddy current loss density can be decreased by 44.8%, which is from 1.51×10^8 to 8.33×10^7 W/m^3.

Meanwhile, to confirm the performance of the alloy gap replacement, eddy current losses on the surfaces that suffer a high amount of gap loss are calculated individually and present in Figure 14. The eddy current loss on those surfaces is reduced by 70% and 40% at gap-winding and side-winding placement, respectively when the switching frequency is 20 kHz. However, the extra eddy current loss from the applied alloy is always a concern and needs to be included in the total eddy current loss comparison. Figure 15 indicates that the reduced gap loss can compensate for the extra eddy current loss from the alloy under different operation conditions with both winding placements. The total eddy current loss can be decreased by 29% and 27% with gap-winding and side-winding placement, respectively by the proposed method at 20 kHz switching frequency conditions. For high frequency condition such as 40 kHz, the eddy current loss on the surfaces can be mitigated by 79% and 38% at gap winding and side winding placement, respectively based on Figure 16. Meanwhile, Figure 17 indicates the total eddy current loss can be reduced by 30% and 20% at gap winding and side winding placement, respectively.

Therefore, the above finite element model results show that this method can significantly reduce the eddy current loss around the gap area. Even including the additional loss of the alloy, the total eddy current loss can still be decreased to 71% and 73% of the previous total value at two winding placements, respectively at 20 kHz switching frequency condition. In terms of the 40 kHz switching frequency condition, the corresponding total eddy current loss of the inductor can be reduced to 70%

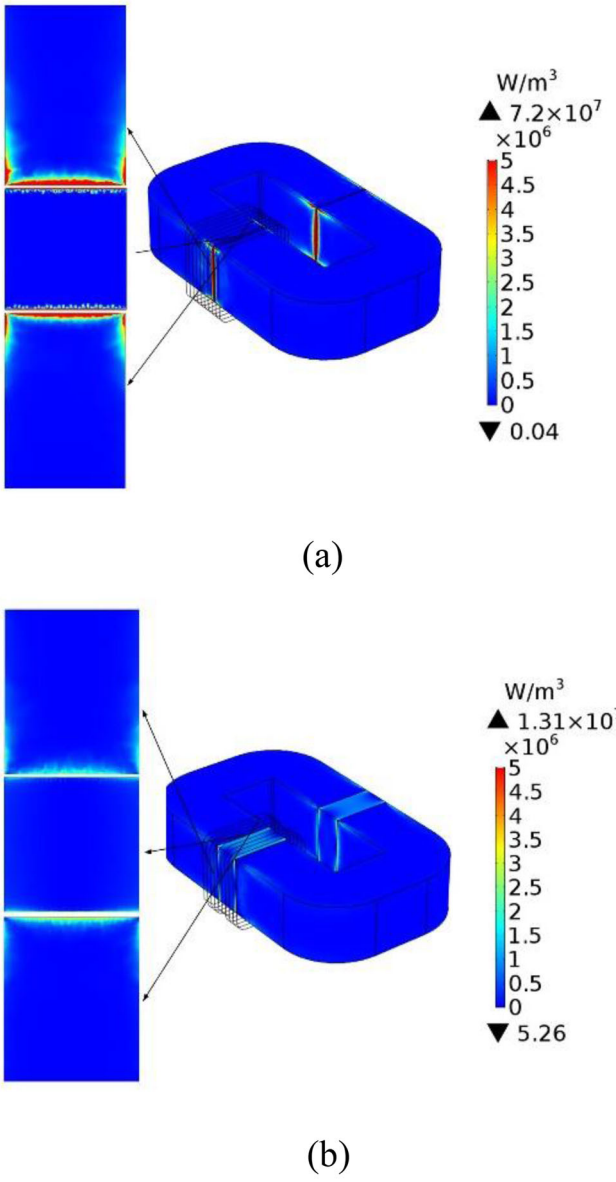

FIGURE 12 Comparison of eddy current loss distribution for the (a) air-gapped and (b) alloy gapped inductors (32 A peak-to-peak ripple current and 40 kHz) at gap winding placement

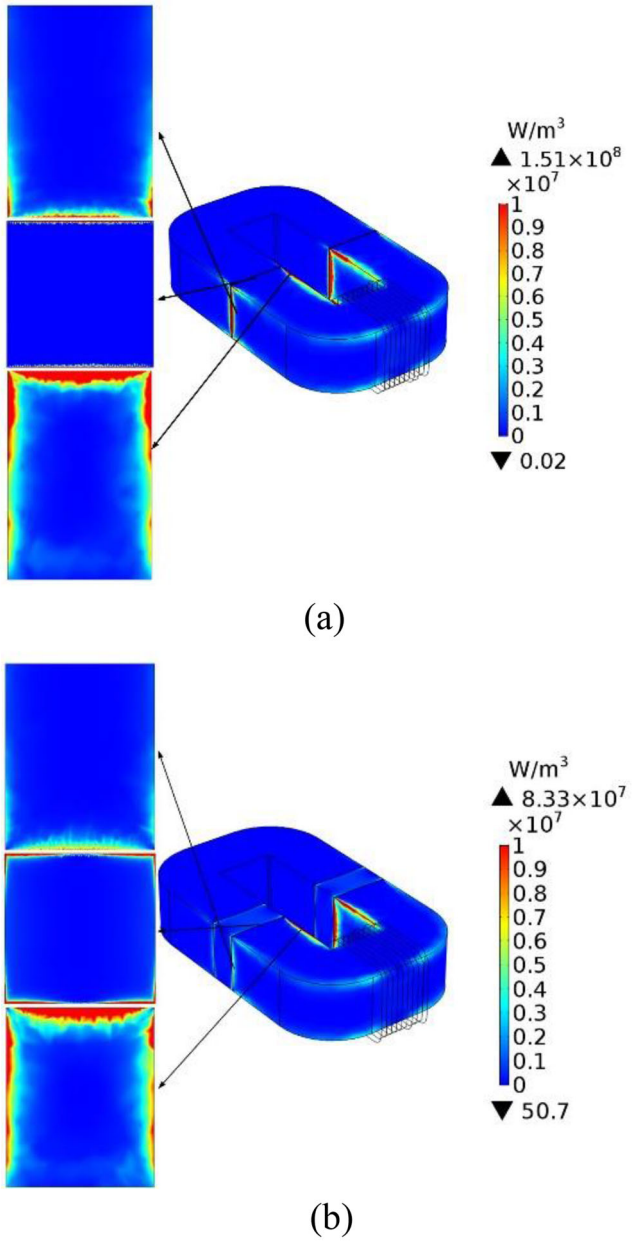

FIGURE 13 Comparison of eddy current loss distribution for the (a) air-gapped and (b) alloy gapped inductors (32 A peak-to-peak ripple current and 40 kHz) at side winding placement

and 82% at gap winding and side winding placement, respectively. Moreover, according to the eddy current loss density distribution comparison in figure 10–14, the more uniformly eddy current loss distribution can be achieved.

4 | FINITE ELEMENT THERMAL MODELLING

The localized hotspot is the direct reflection of the concentrated eddy current loss. Besides, the filter inductor design is eventually thermally limited. Hence, to confirm the effect of the alloy gap replacement on the downsizing of inductor design, the thermal distributions of both inductor designs need to be investigated

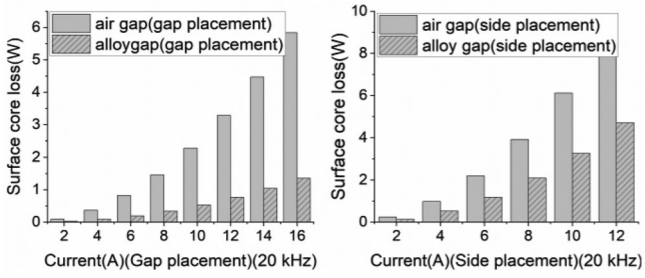

FIGURE 14 Eddy current loss of the outermost surfaces with gap-winding placement (left) and side placement (right) at 20 kHz

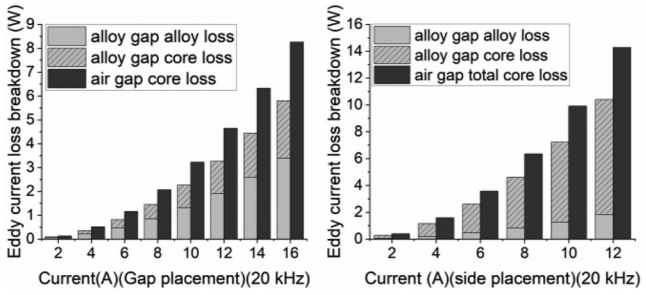

FIGURE 15 Total eddy current loss of gap-winding placement (left) and side-winding placement (right) at 20 kHz

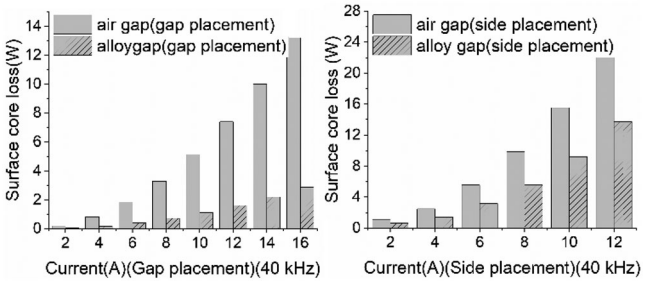

FIGURE 16 Eddy current loss of the outermost surfaces with gap-winding placement (left) and side placement (right) at 40 kHz

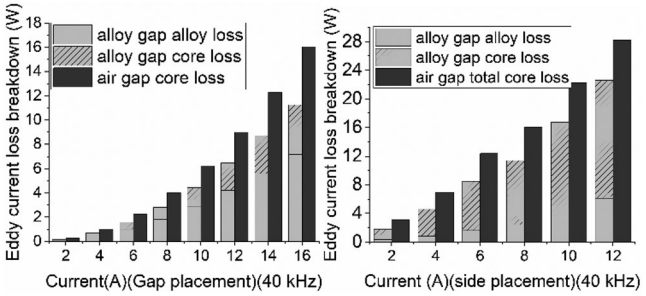

FIGURE 17 Total eddy current loss of gap-winding placement (left) and side-winding placement (right) at 40 kHz

and compared. Since the winding loss is dissipated in the coil instead of the core and has little effect on the core temperature, it is not involved in the thermal model, and the winding coils are only determined as the magnetic source. The hysteresis loss only accounts for a small amount of total core loss and evenly distributes in the whole core; hence, it is calculated separately based on the datasheet instead of simulating in the thermal model.

Two 3D electromagnetic FE models are created, and corresponding eddy current loss distribution results are presented in the previous section. Then the thermal model can be directly modelled and calculated by importing and coupling electromagnetic analysis. To properly model the laminated structure, the method in [2] can obtain a similar thermal result and is chosen as the method to model the thermal behaviour of the proposed inductor design. The nanocrystalline core is defined as several heat sources with constant thermal conductivity instead

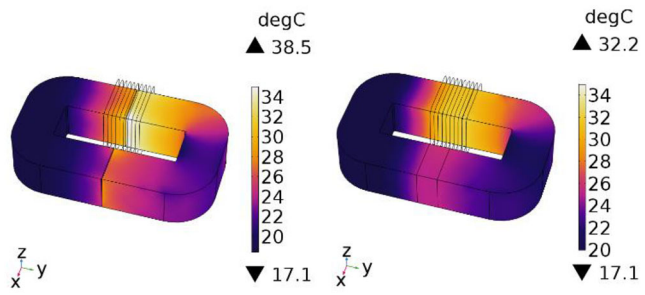

FIGURE 18 FE thermal results of air-gapped (left) and alloy-gapped (right) with one side winding at gap-winding placement (32 A peak-to-peak ripple current and 20 kHz)

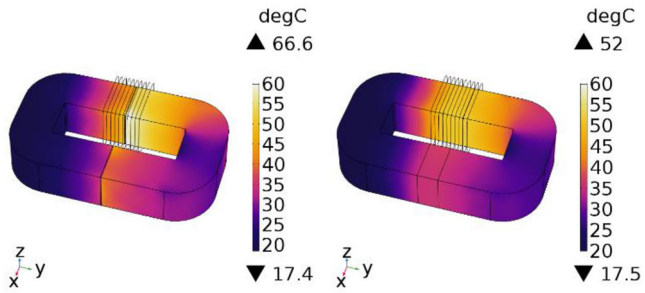

FIGURE 19 FE thermal results of air-gapped (left) and alloy-gapped (right) with one side winding at gap-winding placement (48 A peak-to-peak ripple current and 20 kHz)

of one heat source with anisotropic thermal conductivity to model thermal behaviour around the gap region. A block is set as air-fluid with corresponding default thermal characteristics as the air surrounding the whole inductor simulates the air-forced cooling method. Moreover, based on the eddy current loss results in the previous section, the alloy gapped inductor has better loss reduction performance with gap-winding placement. Therefore, to obtain better thermal performance, only the thermal distribution results with gap-winding placement are presented and discussed.

Different FE thermal results based on different operation conditions and different inductor designs are present in the following figures. Figure 18 shows that the highest hotspot temperature can be reduced by 6.3 °C at 32 A peak-to-peak ripple current condition at 20 kHz, which is the low gap loss condition. When it comes to higher gap loss, which also means higher frequency or higher ripple current, Figures 19 and 20 indicate the hotspot temperature can be reduced by 14.6 and 20.8 °C at 48 A peak-to-peak ripple current and 40 kHz frequency, respectively. For different inductor designs such as two side winding and wider lamination width, Figures 21 and 22 indicate that the proposed method can mitigate the hotspot temperature by 24.1 and 22.4 °C for two sides winding and wider lamination width respectively. FE thermal results indicate that the proposed method can significantly reduce hotspot temperature under different operating conditions and various inductor designs. Moreover, a more uniform temperature distribution is achieved by the proposed method. Hence, the thermally limited inductor can be

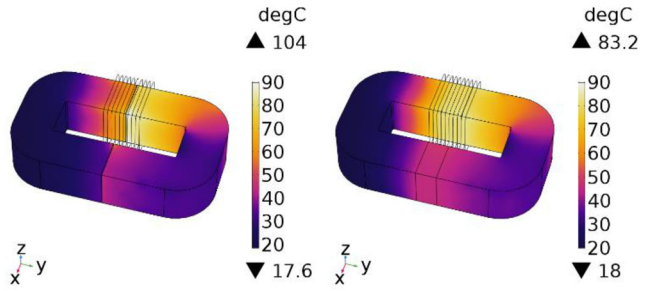

FIGURE 20 FE thermal results of air-gapped (left) and alloy gapped (right) with one side winding at gap-winding placement (32 A peak-to-peak ripple current and 40 kHz)

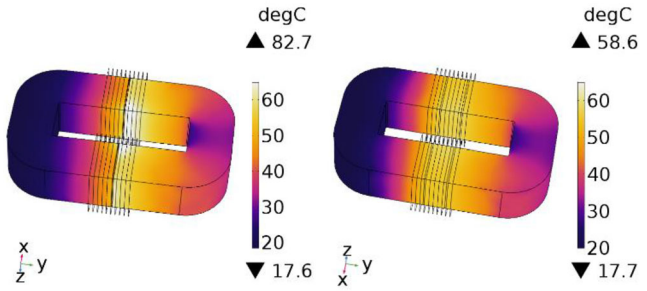

FIGURE 21 FE thermal results of air-gapped (left) and alloy gapped (right) with two side winding at gap-winding placement (32 A peak-to-peak ripple current, 20 kHz and 20 turns)

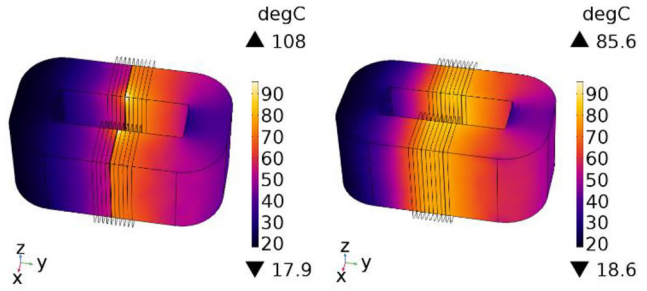

FIGURE 22 FE thermal results of air-gapped (left) and alloy gapped (right) with two side winding at gap-winding placement (32 A peak-to-peak ripple current, 20 kHz, 20 turns and 60 mm lamination width)

predicted to obtain a considerable size reduction through the alloy gap replacement.

5 | EXPERIMENTAL VALIDATION

To confirm the effect of the proposed method, it is necessary to verify the finite element loss model and the thermal model through corresponding experiments. In this study, both the loss experiment and the temperature experiment are only used to verify the accuracy of the finite element model. Therefore, a 3 kW half-bridge inverter test bench was established to simulate the actual working conditions of the filter inductor and verify the two FE models, as shown in Figure 23. Since

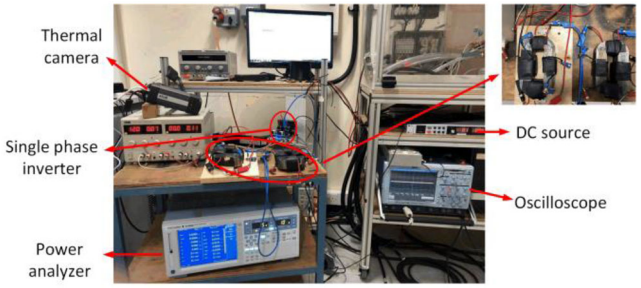

FIGURE 23 Experiment test bench set up

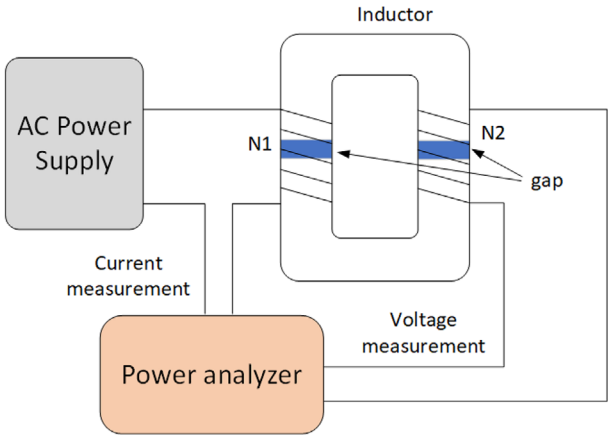

FIGURE 24 Schematic diagram of core loss measurement

the gap loss is not sensitive to low-frequency components, the 50 Hz fundamental wave is set small to obtain better verification results. Attach a suitable thin insulating layer between the alloy block and the nanocrystalline iron core to prevent a short-circuit.

For the FE power loss model, the primary purpose of this study is to evaluate the effect of the alloy gap approach on reducing the concentrated gap loss of nanocrystalline core. Moreover, the alloy gap method is not only effective in reducing gap loss but also in winding loss. Therefore, to minimize the error of the experiment, the focus of the power loss experiment is to compare the measured core loss with the predicted core loss. Moreover, the predicted core loss is composed of the eddy current loss and hysteresis loss. The eddy current loss is directly calculated from the FE power loss model, and the hysteresis loss is based on the datasheet from the manufacture. The schematic diagram of the iron loss measurement method is shown in Figure 24. Then compare the sum of the calculated eddy current loss in the FE loss model and the separately calculated hysteresis loss with the core loss measured in the experiment. Figures 25 and 26 indicate that the measured core loss is almost the same as the predicted core loss under different working conditions. Therefore, the comparison results can verify the finite element power loss model.

As for the temperature experiment, to verify the effect of the alloy gap method in reducing the hot spot temperature in the gap area and whether it can lead to a more uniform

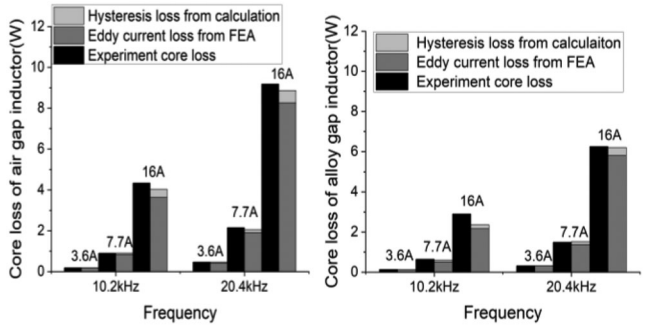

FIGURE 25 Comparison of the measured and predicted core loss of air-gapped inductor (left) and alloy-gapped inductor (right) at gap-winding placement

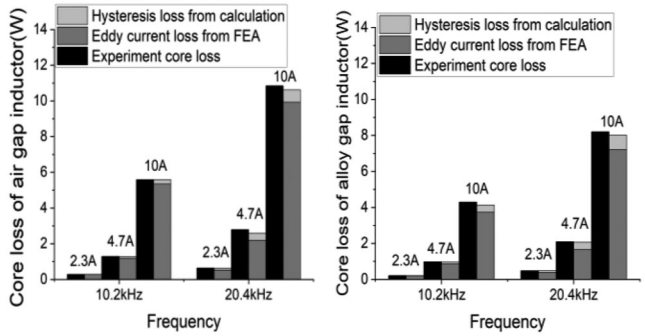

FIGURE 26 Comparison of the measured and predicted core loss of air-gapped inductor (left) and alloy-gapped inductor (right) at side-winding placement

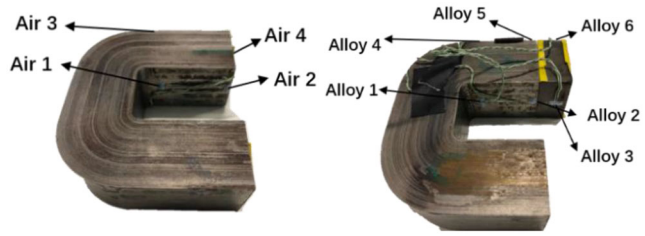

FIGURE 27 Location of the thermocouple of two inductor designs

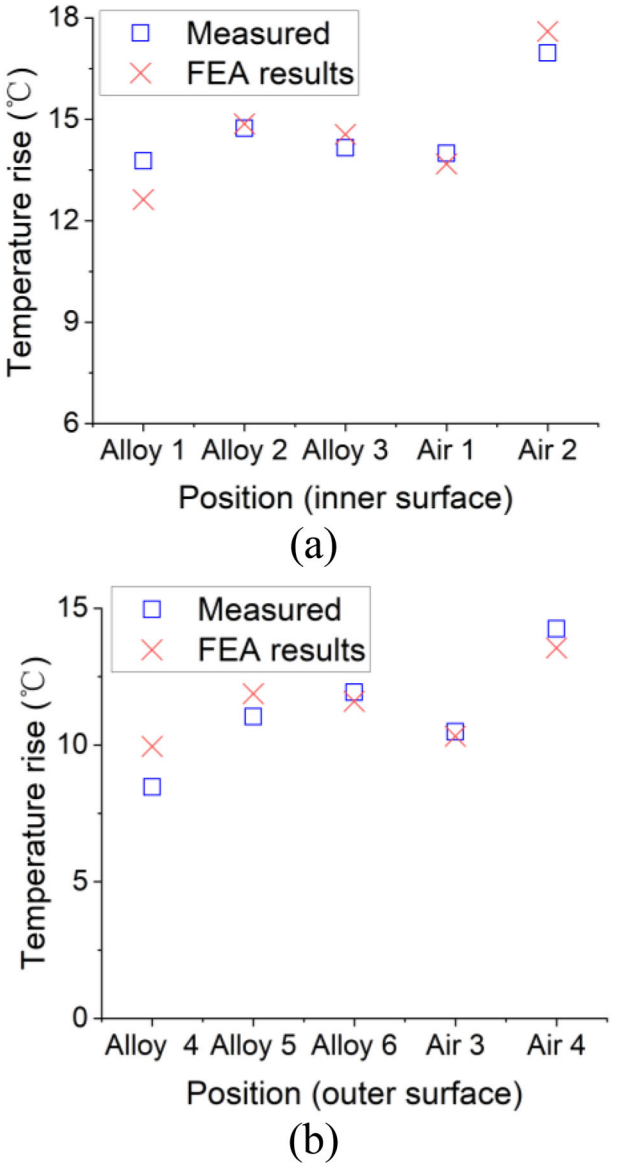

FIGURE 28 Comparison of the measured and predicted temperature rise of air-gapped inductor and alloy-gapped inductor on the (a) inside and (b) outside

temperature distribution. Since [2, 5] both pointed out that a higher temperature has been observed near the gap region. Therefore, to verify the effect of the alloy gap method, thermocouples are placed at different positions, which are close to the gap or away from the gap to measure the temperature as shown in Figure 27. In addition, a suitable bobbin is placed on the iron core to keep the winding and the iron core at an appropriate distance to minimize the effect of the winding temperature. The temperature experiment should be run for at least 90 min under rated operating conditions (32 A peak-to-peak ripple current) to ensure that the measured temperature rise is in a steady state. Figure 28 indicates that the core temperature predicted by the FE thermal model is almost the same as the corresponding point temperature measured in the temperature experiment, whether it is the inner surface or the outer surface. Therefore, the FE thermal model can be validated by temperature rise comparison.

6 | CONCLUSION

An alloy gap replacement is proposed to decrease eddy current loss concentration problems in nanocrystalline cores in this study. The experimentally validated FE power loss model indicates that the eddy current loss of the laminations with the most severe gap loss can achieve 40% and 70% reductions for different winding placements. The total eddy current loss can be limited to 71% with gap placement winding and 73% with side

placement winding. Moreover, for higher frequency conditions such as 40 kHz, the total eddy current loss can be limited to 70% and 80% with gap winding and side winding placement, respectively. The validated thermal model shows that the alloy gap design decreases the highest temperature around the gap and eliminates the localized hotspot leading to more uniform temperature distributions under different operating conditions. The maximum temperature of the hotspot of the higher switching frequency 40 kHz can be decreased by 20.8°C. In terms of the wider lamination width inductor design, the reduction can reach 22.4 °C. For thermally limited inductor design, a considerable size reduction can be expected by the proposed method. Moreover, the alloy gap mitigates the concentrated gap loss by reducing the fringing flux, which means that the winding loss of the nanocrystalline core-based inductor can be reduced as well. The alloy with better core loss characteristics and thermal properties can help to obtain a better power loss and temperature reduction.

Since the higher DC bias condition requires a larger air gap length, which corresponds to a larger alloy gap length. The longer the alloy gap will cause higher the alloy core loss. Based on this reason, this proposed method may not be suitable for higher DC bias applications.

CONFLICT OF INTEREST

The authors declare no conflict of interest.

FUNDING INFORMATION

There are no funders to report for this submission.

DATA AVAILABILITY STATEMENT

The data that support the findings of this study are available from the corresponding author upon reasonable request.

ORCID

Xuan Guo https://orcid.org/0000-0002-9997-0204

REFERENCES

1. Kolar, J.W., Bortis, D., Neumayr, D.: The ideal switch is not enough. In: 2016 28th International Symposium on Power Semiconductor Devices and ICs (ISPSD), Prague, pp. 15–22 (2016) https://doi.org/10.1109/ISPSD.2016.7520767
2. Wang, Y., Calderon-Lopez, G., Forsyth, A.: Thermal management of compact nanocrystalline inductors for power dense converters. In: 2018 IEEE Applied Power Electronics Conference and Exposition (APEC), San Antonio, TX, pp. 2696–2703 (2018) https://doi.org/10.1109/APEC.2018.834139.
3. Fukunaga, H., Eguchi, T., Ohta, Y., Kakehashi, H.: Core loss in amorphous cut cores with air gaps. IEEE Trans. Magn. 25(3), 2694–2698 (1989) https://doi.org/10.1109/20.24510
4. Fukunaga, H., Eguchi, T., Koga, K., Ohta, Y., Kakehashi, H.: High performance cut cores prepared from crystallized Fe-based amorphous ribbon. IEEE Trans. Magn. 26(5), 2008–2010 (1990) https://doi.org/10.1109/20.104600
5. Wang, Y., Calderon-Lopez, G., Forsyth, A.J.: High-frequency gap losses in nanocrystalline cores. IEEE Trans. Power Electron. 32(6), 4683–4690 (2017) https://doi.org/10.1109/TPEL.2016.2594083
6. Jez, R.: Influence of the distributed air gap on the parameters of an industrial inductor. IEEE Trans. Magn. 53(11), 1–5 (2017)
7. Tera, T., Taki, H., Shimizu, T.: Loss reduction of laminated core inductor used in on-board charger for EVs. In: 2014 International Power Electronics Conference (IPEC-Hiroshima 2014 - ECCE ASIA), Hiroshima, pp. 876–882 (2014)
8. Alabakhshizadeh, A., Midtgård, O.: Air gap fringing flux reduction in a high frequency inductor for a solar inverter. In: 2013 IEEE 39th Photovoltaic Specialists Conference (PVSC), Tampa, FL, pp. 2849–2852 (2013)
9. Fletcher, J., Williams, B., Mahmoud, M.: Airgap fringing flux reduction in inductors using open-circuit copper screens. IEE Proc. Electr. Power Appl. 152(4), 990–996 (2005)
10. Zaikin, D.I., Jonasen, S., Mikkelsen, S.L.: An air-gap shape optimization for fringing field Eddy current loss reductions in power magnetics. IEEE Trans. Power Electron. 34(5), 4079–4086 (2019)
11. Winkler, P., Guenther, W.: Using powder materials to replace air-gaps for fringing flux reduction. In: PCIM Europe 2017; International Exhibition and Conference for Power Electronics, Intelligent Motion, Nuremberg, Germany, pp. 1–6 (2017)
12. Guo, X., Ran, L., Tavner, P.: Reducing local concentrated gap loss of a nanocrystalline core by applying alloy gap. 2020 IEEE Energy Conversion Congress and Exposition (ECCE), pp. 3299–3305 (2020)
13. Wang, J., Lin, H., Huang, Y., Huang, L.: Numerical analysis of 3D Eddy current fields in laminated media under various frequencies. IEEE Trans. Magn. 48(2), 267–270 (2012)
14. Neubert, H., Ziske, J., Heimpold, T. Disselnkotter, R.: Homogenization approaches for laminated magnetic cores using the example of transient 3d transformer modeling. In: Proceedings of the 7th European COMSOL Conference, Rotterdam, NL, pp. 23–25 (2013)
15. Kaimori, H., Kameari, A., Fujiwara, K.: FEM computation of magnetic field and iron loss in laminated iron core using homogenization method. IEEE Trans. Magn. 43(4), 1405–1408 (2007)
16. Borchardt, N., Kasper, R., Sauerhering, J., Heinemann, W., Foster, K.: Multilayer air gap winding designs for electric machines: Theory, design, and characterization. J. Eng. 2019(17), 3855–3861 (2019)
17. Mohan, N., Undeland, T., Robbins, W., Power Electronics, Wiley, Hoboken, NJ (2003)
18. Guo, X., Ran, L., Mawby, P., Jia, C., Ng, C., Mckeever, P.: Feasibility study of SiC devices for low voltage converter in a wind power generation system. In: 2018 IEEE International Power Electronics and Application Conference and Exposition (PEAC), Shenzhen, pp. 1–6 (2018)

How to cite this article: Guo X., Ran Li, Tavner P.: Lessening gap loss concentration problems in nanocrystalline cores by alloy gap replacement. J. Eng. 2022, 411–421 (2022). https://doi.org/10.1049/tje2.12127.